

Double-Tag Events in Two-Photon Collisions at LEP

The L3 Collaboration

Abstract

Double-tag events in two-photon collisions are studied using the L3 detector at LEP centre-of-mass energies from $\sqrt{s} = 189$ GeV to 209 GeV. The cross sections of the $e^+e^- \rightarrow e^+e^- \text{hadrons}$ and $\gamma^*\gamma^* \rightarrow \text{hadrons}$ processes are measured as a function of the product of the photon virtualities, $Q^2 = \sqrt{Q_1^2 Q_2^2}$, of the two-photon mass, $W_{\gamma\gamma}$, and of the variable $Y = \ln(W_{\gamma\gamma}^2/Q^2)$. The average photon virtuality is $\langle Q_1^2 \rangle = \langle Q_2^2 \rangle = 16 \text{ GeV}^2$. The results are in agreement with next-to-leading order calculations for the process $\gamma^*\gamma^* \rightarrow q\bar{q}$ in the interval $2 \leq Y \leq 5$. An excess is observed in the interval $5 < Y \leq 7$, corresponding to $W_{\gamma\gamma}$ greater than 40 GeV. This may be interpreted as a contribution of resolved photon QCD processes or the onset of BFKL phenomena.

Submitted to *Phys. Lett. B*

1 Introduction

This letter presents a measurement of cross sections of two-photon collisions: $e^+e^- \rightarrow e^+e^- \text{hadrons}$ obtained with the L3 detector [1] using double-tag events, where both scattered electrons ¹⁾ are detected in the small angle electromagnetic calorimeters. The virtualities of the two photons are defined as $Q_i^2 = 2E_i E_b (1 - \cos \theta_i)$, where E_b is the beam energy, E_i and θ_i are the measured energy and scattering angle of the detected electron ($i = 1$) or positron ($i = 2$). The centre-of-mass energy of the two virtual photons, $W_{\gamma\gamma}$, is related to the e^+e^- centre-of-mass energy, \sqrt{s} , by $W_{\gamma\gamma}^2 \approx sy_1y_2$, with $y_i = 1 - (E_i/E_b) \cos^2(\theta_i/2)$. This is a good approximation in the kinematic range covered by this study, where $W_{\gamma\gamma}^2$ is usually much larger than Q_i^2 . It is convenient to define the dimensionless variable Y :

$$Y = \ln \frac{W_{\gamma\gamma}^2}{Q^2}, \quad Q^2 = \sqrt{Q_1^2 Q_2^2} \quad (1)$$

which depends mainly on the angles of the scattered electrons and allows the combination of the data collected at different values of \sqrt{s} .

Taking advantage of the good energy resolution of the small angle electromagnetic calorimeters, $W_{\gamma\gamma}$ is calculated as the missing mass of the two scattered electrons, W_{ee} . This avoids an unfolding procedure to calculate $W_{\gamma\gamma}$ from the effective mass of the hadrons observed in the detector, W_{vis} , which is the dominant source of systematic uncertainty on the measurement of the $e^+e^- \rightarrow e^+e^- \text{hadrons}$ cross sections for untagged [2,3] and single-tag [4,5] events. However the W_{ee} variable is more strongly affected by QED radiative corrections than W_{vis} .

In perturbation theory, the cross section of the $\gamma^*\gamma^* \rightarrow \text{hadrons}$ process is described in terms of a fixed order expansion in the strong coupling constant, complemented with the DGLAP [6] evolution of the parton density of the photon. All two-to-two leading order (LO) processes, such as $\gamma\gamma \rightarrow q\bar{q}$ (QPM) or, for example, $\gamma g \rightarrow q\bar{q}$ or $\gamma q \rightarrow gq$ (single resolved) and $gg \rightarrow q\bar{q}$ (double resolved), are taken into account in the Monte Carlo generators used to analyse the data. If the virtualities of the two photons are large and comparable, LO processes are expected to be suppressed relative to diagrams where multiple gluons are exchanged between the $q\bar{q}$ dipoles [7] coupling to each virtual photon. Examples of possible diagrams are given in Figure 1. In leading logarithmic approximation, the resummed series of perturbative gluonic ladders can be described by the BFKL equation [8], which predicts a rise in cross sections as a power of $W_{\gamma\gamma}$, as if a “hard Pomeron” [9] was exchanged. The cross section measurement of two virtual photons is considered as a “golden” process to test BFKL dynamics [10]. After our first publication on the double-tag data at $\sqrt{s} = 91$ GeV and 183 GeV [11], an effort was made to improve the QPM calculation by including QCD corrections [12]. The effects of varying the charm mass and the strong coupling constant were studied as well as the contribution of longitudinal photon polarization states [13]. The relative importance of perturbative and non perturbative QCD effects was also addressed by considering Reggeon and Pomeron contributions [14,15]. There are also many efforts to include next-to-leading order (NLO) corrections in the BFKL model [16].

The data, discussed in this letter, were collected at $\sqrt{s} = 189\text{--}209$ GeV and correspond to an integrated luminosity of 617 pb^{-1} , for a luminosity weighted centre-of-mass energy 197.9 GeV. The observed value of Q_i^2 is in the range $4\text{--}44 \text{ GeV}^2$ with an average value of $\langle Q_i^2 \rangle = 16 \text{ GeV}^2$. The kinematic region $E_{1,2} > 40 \text{ GeV}$, $30 \text{ mrad} < \theta_{1,2} < 66 \text{ mrad}$ and $W_{\gamma\gamma} > 5 \text{ GeV}$ is investigated. A study of asymmetric double-tag events ($Q_1^2 \gg Q_2^2$) at $\sqrt{s} = 91 \text{ GeV}$ was previously

¹⁾Electron stands for electron or positron throughout this paper.

reported [17].

2 Event Generators

Two Monte Carlo generators, PHOJET [18] and TWOGAM [19], are used to simulate double-tag two-photon events. Both use the GRV-LO [20] parton density in the photon and include all two-to-two LO $\gamma\gamma$ diagrams. They describe well single-tag events [4].

PHOJET is an event generator for pp, γp and two-photon interactions, based on the Dual Parton Model. The electron-photon vertex for transversely polarized photons [21] is simulated. A transverse momentum cutoff of 2.5 GeV on the outgoing partons is applied to separate soft from hard processes [22]. PHOJET gives also a good description of untagged $\gamma\gamma \rightarrow \text{hadrons}$ events [2]. The electromagnetic coupling constant, α_{em} , in PHOJET is fixed to the value for on-shell photons.

TWOGAM generates three different processes separately: QPM, QCD resolved photon processes and non perturbative soft processes described by the Vector Dominance Model (VDM). The normalization of the QPM process is determined by the quark masses ($m_u = m_d = 0.3$ GeV, $m_s = 0.5$ GeV and $m_c = 1.6$ GeV), that of the VDM process is fixed by our measurement of the cross section of real photons [2], while the normalization of the QCD contribution is adjusted to reproduce the observed number of data events. TWOGAM was recently upgraded to take into account QED soft and hard radiation from initial (ISR) and final state (FSR) electrons. The accuracy of the implementation of QED radiative corrections is checked with the program RADCOR [23], using the channel $e^+e^- \rightarrow e^+e^-\mu^+\mu^-$.

The data are mainly sensitive to initial state radiation which modifies the shape of the Y spectrum. Since the various processes have different Y dependences, the radiative correction affects them differently, as shown in Figure 2a. Here the cross sections are calculated in the generator level within the kinematic region defined above. The variables Q^2 and $W_{\gamma\gamma}$ are calculated from the kinematics of scattered electrons. The relative contributions of QPM, VDM and QCD, as predicted by the TWOGAM program, including QED radiative effects, are given in Figure 2b and listed in Table 1. The VDM contribution is small and almost constant in our kinematical region. The resolved photon QCD contribution is negligible at low values of Y and increases to about 50% at high values.

The dominant backgrounds are $e^+e^- \rightarrow e^+e^-\tau^+\tau^-$ events, simulated by JAMVG [24], and single-tag two-photon hadronic events, where a hadron mimics a scattered electron. Other background processes are simulated by PYTHIA [25] ($e^+e^- \rightarrow \text{hadrons}$), KORALZ [26] ($e^+e^- \rightarrow \tau^+\tau^-$) and KORALW [27] ($e^+e^- \rightarrow W^+W^-$).

All Monte Carlo events are passed through a full detector simulation of the L3 detector which uses the GEANT [28] and the GEISHA [29] packages and are reconstructed in the same way as the data. Time dependent detector inefficiencies, as monitored during the data taking period, are also simulated. The effect of the detector on the generated value of Y , Y_{gen} , is presented in Figure 2c, where the distribution of value reconstructed from the hadronic system, Y_{vis} , is shown in comparison with the quantity Y_{ee} obtained from scattered electrons. The distortion and limited range of the Y_{vis} spectrum, due to the effect of undetected particles, is evident.

3 Event Selection

Double-tag two-photon events are recorded by two independent triggers: the central track trigger [30] and the single- and double-tag energy triggers [31] leading to a total trigger efficiency greater than 99%.

Two-photon hadronic event candidates, $e^+e^- \rightarrow e^+e^- \text{hadrons}$, are selected using the following criteria:

- There must be two identified electrons, forward and backward, in the small angle electromagnetic calorimeters. Each electron is identified as the highest energy cluster in one of the calorimeters, with energy greater than 40 GeV. The scattering angles of the two tagged electrons have to be in the range $30 \text{ mrad} < \theta_{1,2} < 66 \text{ mrad}$. The opening angle between the momentum vectors of the scattered electrons must be smaller than 179.5° , to reject Bhabha events. Figure 3 shows the distributions of E_i/E_b , Q_i^2 , θ_i and $\log(Q_1^2/Q_2^2)$ for scattered electrons. TWOGAM describes the shape of the distributions of θ_i and Q_i^2 better than PHOJET.
- The number of particles, defined as tracks and isolated calorimeter clusters in the polar angle region $20^\circ < \theta < 160^\circ$, must be greater than 5. The tracks are selected by requiring a transverse momentum greater than 100 MeV and a distance of closest approach, in the transverse plane, to the interaction vertex smaller than 10 mm. Isolated energy clusters are required to have energy greater than 100 MeV and no nearby charged track inside a cone of 35 mrad half-opening angle.
- The visible hadronic mass W_{vis} , calculated from the four-vectors of all measured particles, must be greater than 2.5 GeV in order to exclude beam-gas and off-momentum electron backgrounds. The distributions of W_{vis} and of the corresponding variable $Y_{vis} = \ln(W_{vis}^2/\sqrt{Q^2})$ are compared to Monte Carlo distributions in Figure 4a and b.

After these requirements, 491 events are selected with an estimated background of 49 misidentified single-tag events and 32 events from the process $e^+e^- \rightarrow e^+e^-\tau^+\tau^-$. Other background processes are estimated to contribute 6 events. The variable $W_{\gamma\gamma}$ and the corresponding value of Y are calculated from the scattered electron variables, W_{ee} and Y_{ee} , shown in Figure 4c and d. Good agreement is observed with both Monte Carlo generators.

4 Results

The differential cross sections of the $e^+e^- \rightarrow e^+e^- \text{hadrons}$ process with respect to the variables Q^2 , $W_{\gamma\gamma}$ and Y are measured in the kinematic region:

- $E_{1,2} > 40 \text{ GeV}$ and $30 \text{ mrad} < \theta_{1,2} < 66 \text{ mrad}$
- $W_{\gamma\gamma} > 5 \text{ GeV}$

The ranges $10 \text{ GeV}^2 \leq Q^2 \leq 32 \text{ GeV}^2$, $5 \text{ GeV} \leq W_{\gamma\gamma} \leq 100 \text{ GeV}$ and $2 \leq Y \leq 7$ are independently investigated. The cross sections are derived in each interval as:

$$\Delta\sigma = \frac{\Delta N}{\mathcal{L}\varepsilon}\xi \quad (2)$$

where ΔN is the background subtracted number of events, \mathcal{L} is the total integrated luminosity and ε is the selection efficiency. This is the ratio of the selected number of Monte Carlo events after the full detector simulation to the generated number of Monte Carlo events, including QED radiative corrections. An additional multiplicative factor ξ , discussed above and presented in Figure 2a, corrects the effect of QED radiative corrections. The results with and without this correction are given in Table 2 for different bins together with the number of observed events and the selection efficiencies. The size of QED radiative corrections is estimated by TWOGLAM using the relative proportions of the three components after adjusting the QCD component to the data.

The systematic uncertainty on the cross sections due to the selection is 5%. It is dominated by the effect of a variation of the multiplicity cut from 4 to 6 particles. The uncertainty from the background estimation of single-tag events is 3.5% and that due to Monte Carlo statistics amounts to 1%. The uncertainty due to Monte Carlo modelling is estimated as 6.4% by comparing PHOJET and TWOGLAM without QED radiative corrections. To check the implementation of QED radiative corrections, the TWOGLAM predictions for the $e^+e^- \rightarrow e^+e^-\mu^+\mu^-$ process are compared to those of RADCOR. The difference is within 3% which is included as a systematic uncertainty. The different systematic uncertainties are summarised in Table 3. The different contribution from QPM, VDM and QCD as function of Y and $W_{\gamma\gamma}$ gives an additional systematic uncertainty. A 20% variation of the QCD component results into an uncertainty of 0.3% at low values of Y and $W_{\gamma\gamma}$ and of 5.7% at large values. This uncertainty is about 0.5% over the full Q^2 region.

The $e^+e^- \rightarrow e^+e^- \text{hadrons}$ cross sections after the application of QED radiative corrections are compared in Figure 5 to the PHOJET Monte Carlo and to LO and NLO calculations of $\gamma^*\gamma^* \rightarrow q\bar{q}$ [12]. In these calculations the mass of quarks is set to zero and α_{em} is fixed to the value for on-shell photons. The predictions of these models are also listed in Table 4. These calculations describe well the Q^2 dependence of the data. For the $W_{\gamma\gamma}$ and Y distributions, the QPM calculations describe the data except in the last bin, where the experimental cross section exceeds the predictions. Such an excess is expected if the resolved photon QCD processes become important at large Y , as illustrated in Figure 2b. The predictions of PHOJET, which includes the QPM and QCD processes in the framework of the DGLAP equation, also describe the data. A similar behaviour may also be obtained by considering the “hard Pomeron” contribution in the framework of BFKL [15] theories, while LO BFKL calculations were found to exceed the experimental values by a large factor [11].

From the measurement of the $e^+e^- \rightarrow e^+e^- \text{hadrons}$ cross section, σ_{ee} , we extract the two-photon cross section, $\sigma_{\gamma^*\gamma^*}$, by using the transverse photon luminosity function, L_{TT} [21, 32], $\sigma_{ee} = L_{TT}\sigma_{\gamma^*\gamma^*}$. $\sigma_{\gamma^*\gamma^*}$ represents an effective cross section containing contributions from transverse (T) and longitudinal (L) photon polarisations:

$$\sigma_{\gamma^*\gamma^*} = \sigma_{TT} + \epsilon_1\sigma_{LT} + \epsilon_2\sigma_{TL} + \epsilon_1\epsilon_2\sigma_{LL} + \frac{1}{2}\zeta_1\zeta_2 \int \tau_{TT} \cos 2\tilde{\varphi} d\tilde{\varphi} - 4\eta_1\eta_2 \int \tau_{TS} \cos \tilde{\varphi} d\tilde{\varphi} \quad (3)$$

with

$$\zeta_i \sim \eta_i \sim \epsilon_i = \frac{2(1 - y_i)}{1 + (1 - y_i)^2} \quad , \quad \text{when } y_i \ll 1 \quad (4)$$

where $\tilde{\varphi}$ is the angle between the e^+e^- scattering planes in the two-photon centre-of-mass system. Using the GALUGA Monte Carlo program [32], the contribution of the interference terms τ_{TT} and τ_{TS} is found to be negligible for the QPM contribution, when $Y > 3$. In the

kinematical region studied, the average value of ϵ_i is about 0.95. The experimental values of $\sigma_{\gamma^*\gamma^*}$ are presented in Table 5 and Figure 6 in the same ranges considered above with and without QED radiative corrections. The measurements as a function of Q^2 are fitted by the form $f = A/Q^2$, expected by perturbative QCD [10, 14]. The fit reproduces the data well with $A = 81.8 \pm 6.4 \text{ nb/GeV}^2$ and $\chi^2/d.o.f = 1.2/3$. The average value of $\sigma_{\gamma^*\gamma^*}$ in the kinematical region considered is $4.7 \pm 0.4 \text{ nb}$. The NLO calculations [12] predict a decrease of $\sigma_{\gamma^*\gamma^*}$ as a function of $W_{\gamma\gamma}$ or Y , which is inconsistent with the measurements at large values of $W_{\gamma\gamma}$ and Y .

Acknowledgements

We thank M. Przybycien and R. Nisius for pointing out the importance of QED radiative corrections in this process and S. Todorova for numerous discussions about their implementations in the TWOGAM Monte Carlo.

References

- [1] L3 Collab., B. Adeva *et al.*, Nucl. Instr. Meth. **A 289** (1990) 35;
J.A. Bakken *et al.*, Nucl. Instr. Meth. **A 275** (1989) 81;
O. Adriani *et al.*, Nucl. Instr. Meth. **A 302** (1991) 53;
B. Adeva *et al.*, Nucl. Instr. Meth. **A 323** (1992) 109;
K. Deiters *et al.*, Nucl. Instr. Meth. **A 323** (1992) 162;
M. Acciari *et al.*, Nucl. Instr. Meth. **A 351** (1994) 300
- [2] L3 Coll., M. Acciarri *et al.*, Phys. Lett. **B 408** (1997) 450;
L3 Coll., M. Acciarri *et al.*, Preprint CERN-EP/2001-012, Phys. Lett. B accepted
- [3] OPAL Coll., G. Abbiendi *et al.*, Eur. Phys. J. **C 14** (2000) 99
- [4] L3 Coll., M. Acciarri *et al.*, Phys. Lett. **B 436** (1998) 403;
L3 Coll., M. Acciarri *et al.*, Phys. Lett. **B 447** (1999) 147
- [5] OPAL Coll., G. Abbiendi *et al.*, Eur. Phys. J. **C 18** (2000) 15;
ALEPH Coll., D. Barate *et al.*, Phys. Lett. **B 458** (1999) 152;
DELPHI Coll., P. Abreu *et al.*, Z. Phys. **C 69** (1996) 223
- [6] V.N. Gribov and L.N. Lipatov, Sov. J. Nucl. Phys. **15** (1972) 438 and 675;
L.N. Lipatov, Sov. J. Nucl. Phys. **20** (1975) 94;
Yu.L. Dokshitzer, Sov. Phys. JETP **46** (1977) 641;
G. Altarelli and G. Parisi, Nucl. Phys. **B 126** (1977) 298
- [7] H.G. Dosch, T. Gousset and H.J. Pirner, Phys. Rev. **D 57** (1998) 1666
- [8] E.A. Kuraev, L.N. Lipatov and V.S. Fadin, Sov. Phys. JETP **45** (1977) 199;
Ya.Ya. Balitski and L.N. Lipatov, Sov. J. Nucl. Phys. **28** (1978) 822
- [9] A. Donnachie and P.V. Landshoff, Phys. Lett. **B 437** (1998) 408
- [10] J. Bartels, A. De Roeck and H. Lotter, Phys. Lett. **B 389** (1996) 742;
S.J. Brodsky, F. Hautmann and D.E. Soper, Phys. Rev. **D 56** (1997) 6957
- [11] L3 Coll., M. Acciarri *et al.*, Phys. Lett. **B 453** (1999) 333
- [12] M. Cacciari *et al.*, JHEP **102** (2001) 29.
We wish to thank the authors for providing us with the program with theoretical calculations
- [13] J. Bartels, C. Ewerz and R. Staritzbichler, Phys. Lett. **B 492** (2000) 56
- [14] A. Donnachie, H.G. Dosch and M. Rueter, Eur. Phys. J. **C 13** (2000) 141
- [15] J. Kwiecinski and L. Motyka, Eur. Phys. J. **C 18** (2000) 343
- [16] V.S. Fadin and L. N. Lipatov, Phys. Lett. **B 429** (1998) 127;
G. Camici and M. Ciafaloni, Phys. Lett. **B 430** (1998) 349 and references therein;
C.R. Schmidt, Phys. Rev. **D 60** (1999) 74003;
J.R. Forshaw, D.A. Ross and A. Sabio Vera, Phys. Lett. **B 455** (1999) 273;

- S.J. Brodsky *et al.*, JETP Lett. **70** (1999) 15;
 G. Salam, JHEP **9807** (1998) 19;
 M. Ciafaloni, D. Colferai and G.P. Salam, Phys. Rev. **D 60** (1999) 114036;
 M. Ciafaloni and D. Colferai, Phys. Lett. **B 452** (1999) 372;
 R.S. Thorne, Phys. Rev. **D 60** (1999) 54031
- [17] L3 Coll., M. Acciarri *et al.*, Phys. Lett. **B 483** (2000) 373
- [18] PHOJET version 1.05c is used.
 R. Engel, Z. Phys. **C 66** (1995) 203;
 R. Engel and J. Ranft, Phys. Rev. **D 54** (1996) 4244
- [19] TWOGAM version 2.04 is used.
 L. Lönnblad *et al.*, “ $\gamma\gamma$ event generators”, in Physics at LEP2, ed. G. Altarelli, T. Sjöstrand and F. Zwirner, CERN 96-01 (1996), Volume 2, 224.
 We thank our colleagues from DELPHI for making their program available to us
- [20] M. Glück, E. Reya and A. Vogt, Phys. Rev. **D 45** (1992) 3986; Phys. Rev. **D 46** (1992) 1973
- [21] V.M. Budnev *et al.*, Phys. Rep. **C 15** (1975) 181
- [22] J.H. Field, F. Kapusta and L. Poggioli, Phys. Lett. **B 181** (1986) 362; Z. Phys. **C 36** (1987) 121
- [23] F.A. Berends, P.H. Daverveldt and R. Kleiss, Nucl. Phys. **B 253** (1985) 421; Comp. Phys. Comm. **40** (1986) 271
- [24] J.A.M. Vermaseren, Nucl. Phys. **B 229** (1983) 347
- [25] T. Sjöstrand, Comp. Phys. Comm. **82** (1994) 74
- [26] S. Jadach, B.F.L. Ward and Z. Wąs, Comp. Phys. Comm. **79** (1994) 503
- [27] M. Skrzypek *et al.*, Comp. Phys. Comm. **94** (1996) 216;
 M. Skrzypek *et al.*, Phys. Lett. **B 372** (1996) 289
- [28] R. Brun *et al.*, GEANT 3.15 preprint CERN DD/EE/84-1 (Revised 1987)
- [29] H. Fesefeldt, RWTH Aachen report PITHA 85/2 (1985)
- [30] P. Béné *et al.*, Nucl. Inst. Meth. **A 306** (1991) 150
- [31] R. Bizzarri *et al.*, Nucl. Inst. Meth. **A 283** (1989) 799
- [32] G.A. Schuler, Comp. Phys. Comm. **108** (1998) 279.

The L3 Collaboration:

P.Achard,²⁰ O.Adriani,¹⁷ M.Aguilar-Benitez,²⁴ J.Alcaraz,^{24,18} G.Alemanni,²² J.Allaby,¹⁸ A.Aloisio,²⁸ M.G.Alvigi,²⁸ H.Anderhub,⁴⁷ V.P.Andreev,^{6,33} F.Anselmo,⁹ A.Arefiev,²⁷ T.Azmoon,³ T.Aziz,^{10,18} P.Bagnaia,³⁸ A.Bajo,²⁴ G.Baksay,¹⁶ L.Baksay,²⁵ S.V.Baldew,² S.Banerjee,¹⁰ Sw.Banerjee,⁴ A.Barczyk,^{47,45} R.Barillere,¹⁸ P.Bartolini,²² M.Basile,⁹ N.Batalova,⁴⁴ R.Battiston,³² A.Bay,²² F.Becattini,¹⁷ U.Becker,¹⁴ F.Behner,⁴⁷ L.Bellucci,¹⁷ R.Berbeco,³ J.Berdugo,²⁴ P.Berges,¹⁴ B.Bertucci,³² B.L.Betev,⁴⁷ M.Biasini,³² M.Biglietti,²⁸ A.Biland,⁴⁷ J.J.Blaising,⁴ S.C.Blyth,³⁴ G.J.Bobbink,² A.Böhm,¹ L.Boldizsar,¹³ B.Borgia,³⁸ S.Bottai,¹⁷ D.Bourilkov,⁴⁷ M.Bourquin,²⁰ S.Braccini,²⁰ J.G.Branson,⁴⁰ F.Brochu,⁴ A.Buijs,⁴³ J.D.Burger,¹⁴ W.J.Burger,³² X.D.Cai,¹⁴ M.Capell,¹⁴ G.Cara Romeo,⁹ G.Carlino,²⁸ A.Cartacci,¹⁷ J.Casaus,²⁴ F.Cavallari,³⁸ N.Cavallo,³⁵ C.Cecchi,³² M.Cerrada,²⁴ M.Chamizo,²⁰ Y.H.Chang,⁴⁹ M.Chemarin,²³ A.Chen,⁴⁹ G.Chen,⁷ G.M.Chen,⁷ H.F.Chen,²¹ H.S.Chen,⁷ G.Chiefari,²⁸ L.Cifarelli,³⁹ F.Cindolo,⁹ I.Clare,¹⁴ R.Clare,³⁷ G.Coignet,⁴ N.Colino,²⁴ S.Costantini,³⁸ B.de la Cruz,²⁴ S.Cucciarelli,³² J.A.van Dalen,³⁰ R.de Asmundis,²⁸ P.Déglon,²⁰ J.Debreczeni,¹³ A.Degré,⁴ K.Deiters,⁴⁵ D.della Volpe,²⁸ E.Delmeire,²⁰ P.Denes,³⁶ F.DeNotaristefani,³⁸ A.De Salvo,⁴⁷ M.Diemoz,³⁸ M.Dierckxsens,² D.van Dierendonck,² C.Dionisi,³⁸ M.Dittmar,^{47,18} A.Doria,²⁸ M.T.Dova,^{11,†} D.Duchesneau,⁴ P.Duinker,² B.Echenard,²⁰ A.Eline,¹⁸ H.El Mamouni,²³ A.Engler,³⁴ F.J.Eppling,¹⁴ A.Ewers,¹ P.Extermann,²⁰ M.A.Falagan,²⁴ S.Falciano,³⁸ A.Favara,³¹ J.Fay,²³ O.Fedin,³³ M.Felcini,⁴⁷ T.Ferguson,³⁴ H.Fesefeldt,¹ E.Fiandrin,³² J.H.Field,²⁰ F.Filthaut,³⁰ P.H.Fisher,¹⁴ W.Fisher,³⁶ I.Fisk,⁴⁰ G.Forconi,¹⁴ K.Freudenreich,⁴⁷ C.Furetta,²⁶ Yu.Galaktionov,^{27,14} S.N.Ganguli,¹⁰ P.Garcia-Abia,^{5,18} M.Gataullin,³¹ S.Gentile,³⁸ S.Giagu,³⁸ Z.F.Gong,²¹ G.Grenier,²³ O.Grimm,⁴⁷ M.W.Gruenewald,^{8,1} M.Guida,³⁹ R.van Gulik,² V.K.Gupta,³⁶ A.Gurtu,¹⁰ L.J.Gutay,⁴⁴ D.Haas,⁵ D.Hatzifotiadou,⁹ T.Hebbeker,^{8,1} A.Hervé,¹⁸ J.Hirschfelder,³⁴ H.Hofer,⁴⁷ M.Hohlmann,²⁵ G.Holzner,⁴⁷ S.R.Hou,⁴⁹ Y.Hu,³⁰ B.N.Jin,⁷ L.W.Jones,³ P.de Jong,² I.Josa-Mutuberría,²⁴ D.Käfer,¹ M.Kaur,¹⁵ M.N.Kienzle-Focacci,²⁰ J.K.Kim,⁴² J.Kirkby,¹⁸ W.Kittel,^{14,27} A.Klimentov,^{14,27} A.C.König,³⁰ M.Kopal,⁴⁴ V.Koutsenko,^{14,27} M.Kräber,⁴⁷ R.W.Kraemer,³⁴ W.Krenz,¹ A.Krüger,⁴⁶ A.Kunin,¹⁴ P.Ladron de Guevara,²⁴ I.Laktineh,²³ G.Landi,¹⁷ M.Lebeau,¹⁸ A.Lebedev,¹⁴ P.Lebun,²³ P.Lecomte,⁴⁷ P.Lecoq,¹⁸ P.Le Coultre,⁴⁷ J.M.Le Goff,¹⁸ R.Leiste,⁴⁶ P.Levtchenko,³³ C.Li,²¹ S.Likhoded,⁴⁶ C.H.Lin,⁴⁹ W.T.Lin,⁴⁹ F.L.Linde,² L.Lista,²⁸ Z.A.Liu,⁷ W.Lohmann,⁴⁶ E.Longo,³⁸ Y.S.Lu,⁷ K.Lübelsmeyer,¹ C.Luci,³⁸ L.Luminari,³⁸ W.Lustermann,⁴⁷ W.G.Ma,²¹ L.Malgeri,²⁰ A.Malinin,²⁷ C.Maña,²⁴ D.Mangeol,³⁰ J.Mans,³⁶ J.P.Martin,²³ F.Marzano,³⁸ K.Mazumdar,¹⁰ R.R.McNeil,⁶ S.Mele,^{18,28} L.Merola,²⁸ M.Meschini,¹⁷ W.J.Metzger,³⁰ A.Mihul,¹² H.Milcent,¹⁸ G.Mirabelli,³⁸ J.Mnich,¹ G.B.Mohanty,¹⁰ G.S.Muanza,²³ A.J.M.Muijs,² B.Musicar,⁴⁰ M.Musy,³⁸ S.Nagy,¹⁶ S.Natale,²⁰ M.Napolitano,²⁸ F.Nessi-Tedaldi,⁴⁷ H.Newman,³¹ T.Niessen,¹ A.Nisati,³⁸ H.Nowak,⁴⁶ R.Oferzynski,⁴⁷ G.Organtini,³⁸ C.Palomares,¹⁸ D.Pandoulas,²⁸ P.Paolucci,²⁸ R.Paramatti,³⁸ G.Passaleva,¹⁷ S.Patricelli,²⁸ T.Paul,¹¹ M.Pauluzzi,³² C.Paus,¹⁴ F.Pauss,⁴⁷ M.Pedace,³⁸ S.Pensotti,²⁶ D.Perret-Gallix,⁴ B.Petersen,³⁰ D.Piccolo,²⁸ F.Pierella,⁹ M.Pioppi,³² P.A.Piroué,³⁶ E.Pistoiesi,²⁶ V.Plyaskin,²⁷ M.Pohl,²⁰ V.Pojidaev,¹⁷ J.Pothier,¹⁸ D.O.Prokofiev,⁴⁴ D.Prokofiev,³³ J.Quartieri,³⁹ G.Rahal-Callot,⁴⁷ M.A.Rahaman,¹⁰ P.Raics,¹⁶ N.Raja,¹⁰ R.Ramelli,⁴⁷ P.G.Rancoita,²⁶ R.Ranieri,¹⁷ A.Raspereza,⁴⁶ P.Razis,²⁹ D.Ren,⁴⁷ M.Rescigno,³⁸ S.Reucroft,¹¹ S.Riemann,⁴⁶ K.Riles,³ B.P.Roe,³ L.Romero,²⁴ A.Rosca,⁸ S.Rosier-Lees,⁴ S.Roth,¹ C.Rosenbleck,¹ B.Roux,³⁰ J.A.Rubio,¹⁸ G.Ruggiero,¹⁷ H.Rykaczewski,⁴⁷ A.Sakharov,⁴⁷ S.Saremi,⁶ S.Sarkar,³⁸ J.Salicio,¹⁸ E.Sanchez,²⁴ M.P.Sanders,³⁰ C.Schäfer,¹⁸ V.Schegelsky,³³ S.Schmidt-Kaerst,¹ D.Schmitz,¹ H.Schopper,⁴⁸ D.J.Schotanus,³⁰ G.Schwering,¹ C.Sciacca,²⁸ L.Servoli,³² S.Shevchenko,³¹ N.Shivarov,⁴¹ V.Shoutko,¹⁴ E.Shumilov,²⁷ A.Shvorob,³¹ T.Siedenbun,¹ D.Son,⁴² P.Spillantini,¹⁷ M.Steuer,¹⁴ D.P.Stickland,³⁶ B.Stoyanov,⁴¹ A.Straessner,¹⁸ K.Sudhakar,¹⁰ G.Sultanov,⁴¹ L.Z.Sun,²¹ S.Sushkov,⁸ H.Suter,⁴⁷ J.D.Swain,¹¹ Z.Szillasi,^{25,¶} X.W.Tang,⁷ P.Tarjan,¹⁶ L.Tauscher,⁵ L.Taylor,¹¹ B.Tellili,²³ D.Teyssier,²³ C.Timmermans,³⁰ Samuel C.C.Ting,¹⁴ S.M.Ting,¹⁴ S.C.Tonwar,^{10,18} J.Tóth,¹³ C.Tully,³⁶ K.L.Tung,⁷ J.Ulbricht,⁴⁷ E.Valente,³⁸ R.T.Van de Walle,³⁰ V.Veszpremi,²⁵ G.Vesztergombi,¹³ I.Vetlitsky,²⁷ D.Vicinanza,³⁹ G.Viertel,⁴⁷ S.Villa,³⁷ M.Vivargent,⁴ S.Vlachos,⁵ I.Vodopianov,³³ H.Vogel,³⁴ H.Vogt,⁴⁶ I.Vorobiev,³⁴²⁷ A.A.Vorobyov,³³ M.Wadhwa,⁵ W.Wallraff,¹ X.L.Wang,²¹ Z.M.Wang,²¹ M.Weber,¹ P.Wienemann,¹ H.Wilkens,³⁰ S.Wynhoff,³⁶ L.Xia,³¹ Z.Z.Xu,²¹ J.Yamamoto,³ B.Z.Yang,²¹ C.G.Yang,⁷ H.J.Yang,³ M.Yang,⁷ S.C.Yeh,⁵⁰ An.Zalite,³³ Yu.Zalite,³³ Z.P.Zhang,²¹ J.Zhao,²¹ G.Y.Zhu,⁷ R.Y.Zhu,³¹ H.L.Zhuang,⁷ A.Zichichi,^{9,18,19} G.Zilizi,^{25,¶} B.Zimmermann,⁴⁷ M.Zöller.¹

- 1 I. Physikalisches Institut, RWTH, D-52056 Aachen, FRG[§]
 - III. Physikalisches Institut, RWTH, D-52056 Aachen, FRG[§]
 - 2 National Institute for High Energy Physics, NIKHEF, and University of Amsterdam, NL-1009 DB Amsterdam, The Netherlands
 - 3 University of Michigan, Ann Arbor, MI 48109, USA
 - 4 Laboratoire d'Annecy-le-Vieux de Physique des Particules, LAPP, IN2P3-CNRS, BP 110, F-74941 Annecy-le-Vieux CEDEX, France
 - 5 Institute of Physics, University of Basel, CH-4056 Basel, Switzerland
 - 6 Louisiana State University, Baton Rouge, LA 70803, USA
 - 7 Institute of High Energy Physics, IHEP, 100039 Beijing, China[△]
 - 8 Humboldt University, D-10099 Berlin, FRG[§]
 - 9 University of Bologna and INFN-Sezione di Bologna, I-40126 Bologna, Italy
 - 10 Tata Institute of Fundamental Research, Mumbai (Bombay) 400 005, India
 - 11 Northeastern University, Boston, MA 02115, USA
 - 12 Institute of Atomic Physics and University of Bucharest, R-76900 Bucharest, Romania
 - 13 Central Research Institute for Physics of the Hungarian Academy of Sciences, H-1525 Budapest 114, Hungary[‡]
 - 14 Massachusetts Institute of Technology, Cambridge, MA 02139, USA
 - 15 Panjab University, Chandigarh 160 014, India.
 - 16 KLTE-ATOMKI, H-4010 Debrecen, Hungary[¶]
 - 17 INFN Sezione di Firenze and University of Florence, I-50125 Florence, Italy
 - 18 European Laboratory for Particle Physics, CERN, CH-1211 Geneva 23, Switzerland
 - 19 World Laboratory, FBLJA Project, CH-1211 Geneva 23, Switzerland
 - 20 University of Geneva, CH-1211 Geneva 4, Switzerland
 - 21 Chinese University of Science and Technology, USTC, Hefei, Anhui 230 029, China[△]
 - 22 University of Lausanne, CH-1015 Lausanne, Switzerland
 - 23 Institut de Physique Nucléaire de Lyon, IN2P3-CNRS, Université Claude Bernard, F-69622 Villeurbanne, France
 - 24 Centro de Investigaciones Energéticas, Medioambientales y Tecnológicas, CIEMAT, E-28040 Madrid, Spain^b
 - 25 Florida Institute of Technology, Melbourne, FL 32901, USA
 - 26 INFN-Sezione di Milano, I-20133 Milan, Italy
 - 27 Institute of Theoretical and Experimental Physics, ITEP, Moscow, Russia
 - 28 INFN-Sezione di Napoli and University of Naples, I-80125 Naples, Italy
 - 29 Department of Physics, University of Cyprus, Nicosia, Cyprus
 - 30 University of Nijmegen and NIKHEF, NL-6525 ED Nijmegen, The Netherlands
 - 31 California Institute of Technology, Pasadena, CA 91125, USA
 - 32 INFN-Sezione di Perugia and Università Degli Studi di Perugia, I-06100 Perugia, Italy
 - 33 Nuclear Physics Institute, St. Petersburg, Russia
 - 34 Carnegie Mellon University, Pittsburgh, PA 15213, USA
 - 35 INFN-Sezione di Napoli and University of Potenza, I-85100 Potenza, Italy
 - 36 Princeton University, Princeton, NJ 08544, USA
 - 37 University of California, Riverside, CA 92521, USA
 - 38 INFN-Sezione di Roma and University of Rome, "La Sapienza", I-00185 Rome, Italy
 - 39 University and INFN, Salerno, I-84100 Salerno, Italy
 - 40 University of California, San Diego, CA 92093, USA
 - 41 Bulgarian Academy of Sciences, Central Lab. of Mechatronics and Instrumentation, BU-1113 Sofia, Bulgaria
 - 42 The Center for High Energy Physics, Kyungpook National University, 702-701 Taegu, Republic of Korea
 - 43 Utrecht University and NIKHEF, NL-3584 CB Utrecht, The Netherlands
 - 44 Purdue University, West Lafayette, IN 47907, USA
 - 45 Paul Scherrer Institut, PSI, CH-5232 Villigen, Switzerland
 - 46 DESY, D-15738 Zeuthen, FRG
 - 47 Eidgenössische Technische Hochschule, ETH Zürich, CH-8093 Zürich, Switzerland
 - 48 University of Hamburg, D-22761 Hamburg, FRG
 - 49 National Central University, Chung-Li, Taiwan, China
 - 50 Department of Physics, National Tsing Hua University, Taiwan, China
- § Supported by the German Bundesministerium für Bildung, Wissenschaft, Forschung und Technologie
- ‡ Supported by the Hungarian OTKA fund under contract numbers T019181, F023259 and T024011.
- ¶ Also supported by the Hungarian OTKA fund under contract number T026178.
- ^b Supported also by the Comisión Interministerial de Ciencia y Tecnología.
- [‡] Also supported by CONICET and Universidad Nacional de La Plata, CC 67, 1900 La Plata, Argentina.
- [△] Supported by the National Natural Science Foundation of China.

$\Delta Q^2(\text{GeV}^2)$	10 – 14	14 – 18	18 – 24	24 – 32
QPM	0.778	0.844	0.890	0.919
VDM	0.079	0.061	0.051	0.049
QCD	0.143	0.095	0.059	0.032
$\Delta W_{\gamma\gamma}(\text{GeV})$	5 – 10	10 – 20	20 – 40	40 – 100
QPM	0.924	0.885	0.740	0.466
VDM	0.071	0.063	0.079	0.084
QCD	0.005	0.052	0.181	0.450
ΔY	2.0 – 2.5	2.5 – 3.5	3.5 – 5.0	5.0 – 7.0
QPM	0.913	0.866	0.724	0.443
VDM	0.069	0.069	0.081	0.091
QCD	0.018	0.065	0.195	0.466

Table 1: Fractional contributions of the three processes, QPM, VDM, and QCD in different Q^2 , $W_{\gamma\gamma}$ and Y intervals as predicted by the TWO GAM Monte Carlo including QED radiative corrections.

ΔQ^2 (GeV ²)	$\langle Q^2 \rangle$ (GeV ²)	Events	ϵ	Before Radiative corrections $d\sigma_{ee}/dQ^2$ (pb/GeV ²)	After Radiative corrections $d\sigma_{ee}/dQ^2$ (pb/GeV ²)
10 – 14	12.0	128.5 \pm 12.4	0.58	0.0898 \pm 0.0087 \pm 0.0081	0.0718 \pm 0.0070 \pm 0.0061 \pm 0.0022
14 – 18	15.9	102.0 \pm 11.2	0.68	0.0612 \pm 0.0067 \pm 0.0055	0.0522 \pm 0.0057 \pm 0.0044 \pm 0.0016
18 – 24	20.5	81.3 \pm 9.8	0.74	0.0298 \pm 0.0036 \pm 0.0027	0.0273 \pm 0.0033 \pm 0.0023 \pm 0.0008
24 – 32	27.0	24.8 \pm 5.5	0.77	0.0065 \pm 0.0014 \pm 0.0006	0.0066 \pm 0.0014 \pm 0.0006 \pm 0.0002
$\Delta W_{\gamma\gamma}$ (GeV)	$\langle W_{\gamma\gamma} \rangle$ (GeV)	Events	ϵ	Before Radiative corrections $d\sigma_{ee}/dW_{\gamma\gamma}$ (pb/GeV)	After Radiative corrections $d\sigma_{ee}/dW_{\gamma\gamma}$ (pb/GeV)
5 – 10	7.2	67.3 \pm 8.7	0.37	0.0594 \pm 0.0076 \pm 0.0053	0.0747 \pm 0.0096 \pm 0.0063 \pm 0.0023
10 – 20	13.9	135.4 \pm 12.6	0.66	0.0332 \pm 0.0031 \pm 0.0030	0.0263 \pm 0.0024 \pm 0.0022 \pm 0.0008
20 – 40	27.9	102.1 \pm 11.1	0.72	0.0114 \pm 0.0012 \pm 0.0010	0.0062 \pm 0.0007 \pm 0.0005 \pm 0.0003
40 – 100	61.6	65.1 \pm 9.8	0.67	0.0026 \pm 0.0004 \pm 0.0002	0.0014 \pm 0.0002 \pm 0.0001 \pm 0.0001
ΔY	$\langle Y \rangle$	Events	ϵ	Before Radiative corrections $d\sigma_{ee}/dY$ (pb)	After Radiative corrections $d\sigma_{ee}/dY$ (pb)
2.0 – 2.5	2.2	51.6 \pm 7.9	0.52	0.322 \pm 0.049 \pm 0.029	0.315 \pm 0.048 \pm 0.027 \pm 0.009
2.5 – 3.5	2.9	115.6 \pm 11.4	0.73	0.258 \pm 0.025 \pm 0.023	0.184 \pm 0.018 \pm 0.016 \pm 0.006
3.5 – 5.0	4.2	109.4 \pm 11.6	0.74	0.160 \pm 0.017 \pm 0.014	0.085 \pm 0.009 \pm 0.007 \pm 0.004
5.0 – 7.0	5.9	53.7 \pm 8.9	0.63	0.069 \pm 0.011 \pm 0.006	0.037 \pm 0.006 \pm 0.003 \pm 0.002

Table 2: Number of events, selection efficiencies, ϵ , and differential cross sections $d\sigma(e^+e^- \rightarrow e^+e^-hadrons)/dQ^2$, $d\sigma(e^+e^- \rightarrow e^+e^-hadrons)/dW_{\gamma\gamma}$ and $d\sigma(e^+e^- \rightarrow e^+e^-hadrons)/dY$. All measurements are given before and after applying QED radiative corrections. The first uncertainty is statistical and the second systematic. The third uncertainty represents the effect from QED radiative corrections, including the 3% from Table 3.

Selection procedure	5.0%
Background estimation	3.5%
Monte Carlo statistics	1.0%
Monte Carlo modelling	6.4%
QED radiative correction	3.0%

Table 3: Contributions to the total systematic uncertainties on the measured cross sections.

ΔQ^2 (GeV ²)	LO $\gamma^*\gamma^* \rightarrow q\bar{q}$ $d\sigma_{ee}/dQ^2$ (pb/GeV ²)	NLO $\gamma^*\gamma^* \rightarrow q\bar{q}$ $d\sigma_{ee}/dQ^2$ (pb/GeV ²)	PHOJET $d\sigma_{ee}/dQ^2$ (pb/GeV ²)
10 – 14	0.0596	0.0619	0.0623
14 – 18	0.0547	0.0545	0.0587
18 – 24	0.0285	0.0279	0.0320
24 – 32	0.0083	0.0079	0.0100
$\Delta W_{\gamma\gamma}$ (GeV)	LO $\gamma^*\gamma^* \rightarrow q\bar{q}$ $d\sigma_{ee}/dW_{\gamma\gamma}$ (pb/GeV)	NLO $\gamma^*\gamma^* \rightarrow q\bar{q}$ $d\sigma_{ee}/dW_{\gamma\gamma}$ (pb/GeV)	PHOJET $d\sigma_{ee}/dW_{\gamma\gamma}$ (pb/GeV)
5 – 10	0.0831	0.0786	0.0509
10 – 20	0.0263	0.0269	0.0359
20 – 40	0.0044	0.0052	0.0094
40 – 100	0.0003	0.0004	0.0010
ΔY	LO $\gamma^*\gamma^* \rightarrow q\bar{q}$ $d\sigma_{ee}/dY$ (pb)	NLO $\gamma^*\gamma^* \rightarrow q\bar{q}$ $d\sigma_{ee}/dY$ (pb)	PHOJET $d\sigma_{ee}/dY$ (pb)
2.0 – 2.5	0.334	0.338	0.356
2.5 – 3.5	0.171	0.181	0.258
3.5 – 5.0	0.052	0.063	0.115
5.0 – 7.0	0.006	0.009	0.023

Table 4: Predictions of LO and NLO $\gamma^*\gamma^* \rightarrow q\bar{q}$ calculations and the PHOJET Monte Carlo generator as a function of Q^2 , $W_{\gamma\gamma}$ and Y .

ΔQ^2 (GeV ²)	$\langle Q^2 \rangle$ (GeV ²)	Before Radiative corrections $\sigma_{\gamma^*\gamma^*}$ (nb)	After Radiative corrections $\sigma_{\gamma^*\gamma^*}$ (nb)
10 – 14	12.0	$8.11 \pm 0.79 \pm 0.73$	$6.49 \pm 0.64 \pm 0.55 \pm 0.20$
14 – 18	15.9	$5.68 \pm 0.62 \pm 0.51$	$4.84 \pm 0.53 \pm 0.41 \pm 0.15$
18 – 24	20.5	$4.94 \pm 0.60 \pm 0.45$	$4.54 \pm 0.55 \pm 0.39 \pm 0.14$
24 – 32	27.0	$3.36 \pm 0.74 \pm 0.30$	$3.38 \pm 0.74 \pm 0.29 \pm 0.10$
$\Delta W_{\gamma\gamma}$ (GeV)	$\langle W_{\gamma\gamma} \rangle$ (GeV)	Before Radiative corrections $\sigma_{\gamma^*\gamma^*}$ (nb)	After Radiative corrections $\sigma_{\gamma^*\gamma^*}$ (nb)
5 – 10	7.2	$5.04 \pm 0.65 \pm 0.45$	$6.34 \pm 0.82 \pm 0.54 \pm 0.19$
10 – 20	13.9	$6.65 \pm 0.62 \pm 0.60$	$5.27 \pm 0.49 \pm 0.45 \pm 0.16$
20 – 40	27.9	$6.84 \pm 0.74 \pm 0.62$	$3.71 \pm 0.40 \pm 0.32 \pm 0.16$
40 – 100	61.6	$9.99 \pm 1.50 \pm 0.90$	$5.24 \pm 0.79 \pm 0.45 \pm 0.34$
ΔY	$\langle Y \rangle$	Before Radiative corrections $\sigma_{\gamma^*\gamma^*}$ (nb)	After Radiative corrections $\sigma_{\gamma^*\gamma^*}$ (nb)
2.0 – 2.5	2.2	$5.78 \pm 0.88 \pm 0.52$	$5.65 \pm 0.86 \pm 0.48 \pm 0.17$
2.5 – 3.5	2.9	$6.85 \pm 0.68 \pm 0.62$	$4.90 \pm 0.48 \pm 0.42 \pm 0.16$
3.5 – 5.0	4.2	$7.52 \pm 0.80 \pm 0.68$	$3.99 \pm 0.42 \pm 0.34 \pm 0.19$
5.0 – 7.0	5.9	$10.9 \pm 1.82 \pm 0.98$	$5.82 \pm 0.97 \pm 0.49 \pm 0.37$

Table 5: The two-photon cross section, $\sigma_{\gamma^*\gamma^*}$, before and after applying QED radiative corrections, as a function of Q^2 , $W_{\gamma\gamma}$ and Y . The first uncertainty is statistical and the second systematic. The third uncertainty represents the effect from QED radiative corrections, including the 3% from Table 3.

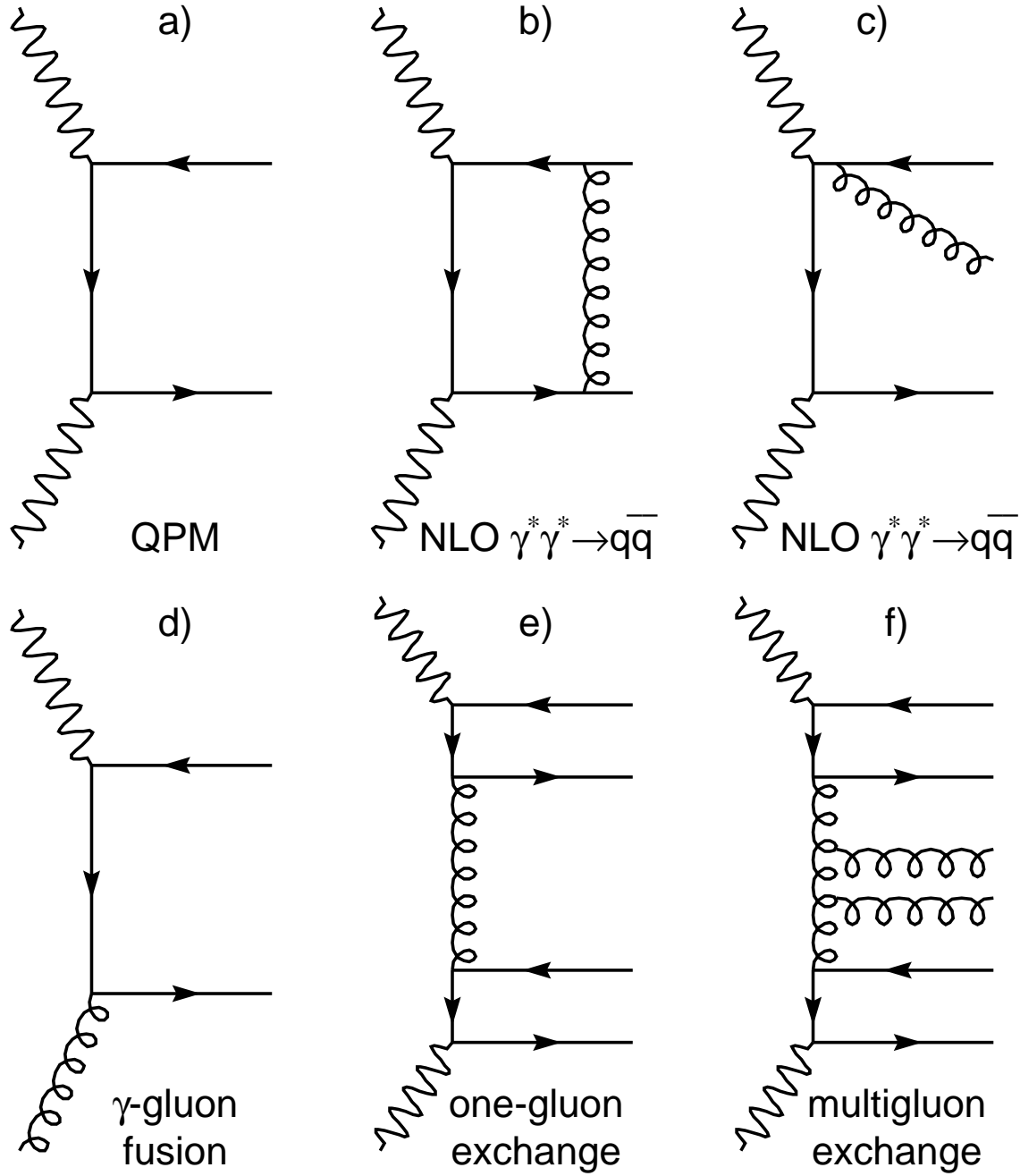


Figure 1: Examples of diagrams contributing to the process $\gamma^* \gamma^* \rightarrow \text{hadrons}$: a) QPM, b) and c) $\mathcal{O}(\alpha_s)$ QCD corrections to the QPM diagram, d) photon-gluon fusion, e) one-gluon exchange and f) multigluon ladder exchange.

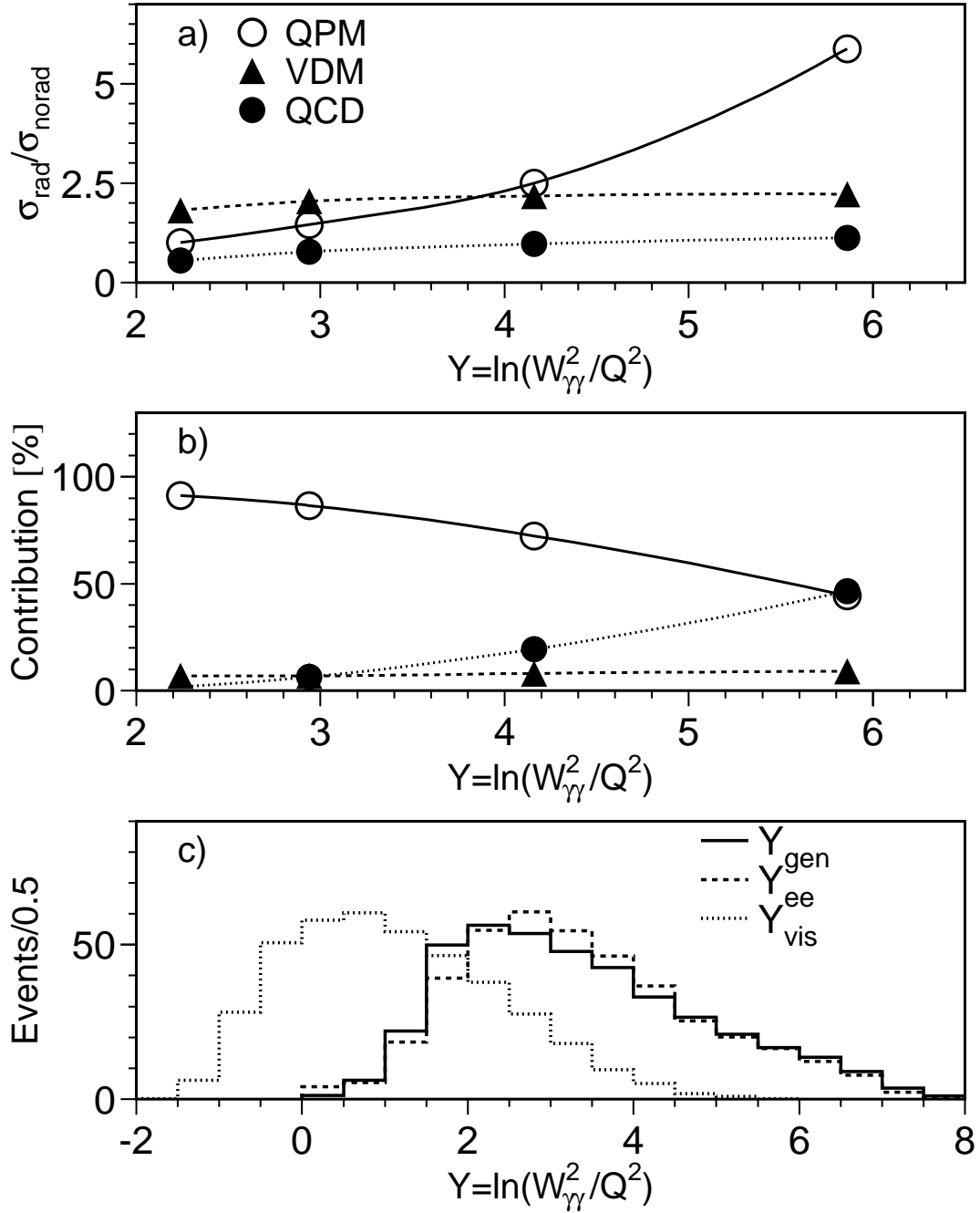


Figure 2: a) QED radiative corrections as a function of the variable Y , for QPM, VDM and QCD processes separately; b) the relative contributions of QPM, VDM and QCD processes in the TWOGAM Monte Carlo with QED radiative corrections included and c) Y determined using W_{vis} or W_{ee} compared to the generated value, Y_{gen} . Lines in a) and b) are drawn to guide the eye.

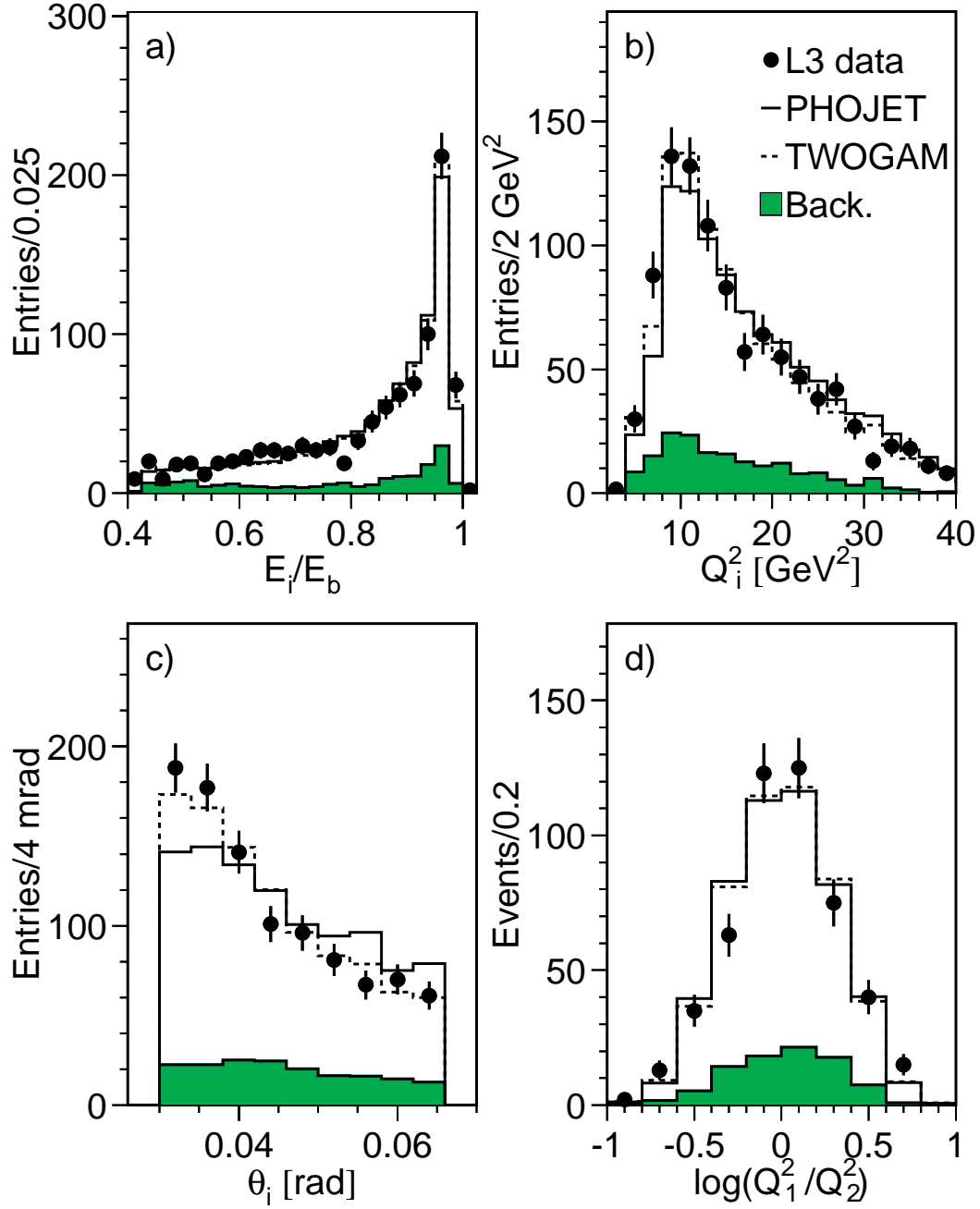


Figure 3: Distributions of a) E_i/E_b , b) Q_i^2 , c) θ_i and d) $\log(Q_1^2/Q_2^2)$ for scattered electrons. The data are compared to Monte Carlo predictions, normalised to the total number of events in the data. The background is mainly due to $e^+e^- \rightarrow e^+e^-\tau^+\tau^-$ and misidentified single-tag two-photon hadronic events.

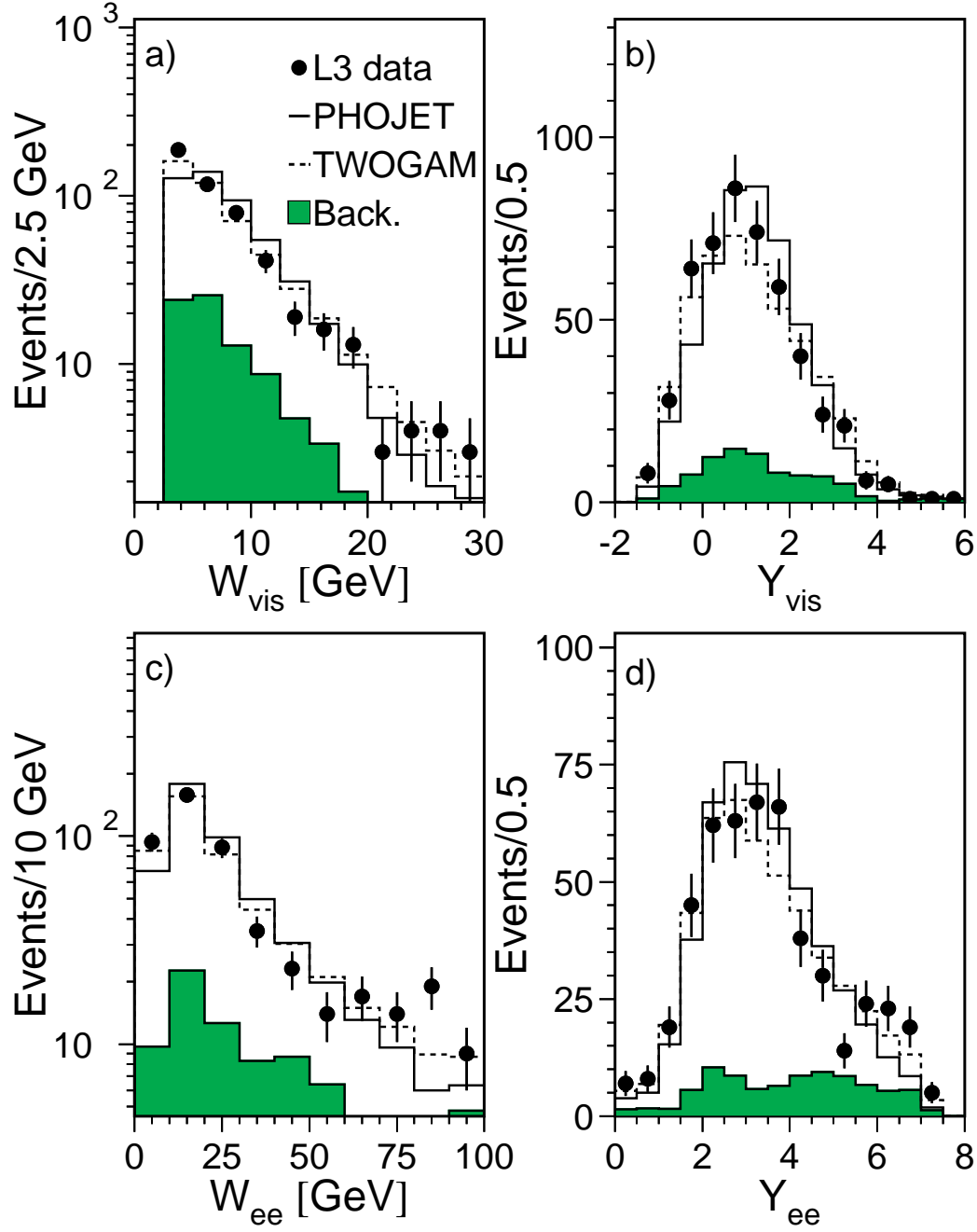


Figure 4: Distributions of a) the effective mass of the detected particles, W_{vis} , b) Y_{vis} , c) the missing mass of the two scattered electrons, W_{ee} and d) the variable Y_{ee} . The range of W_{vis} and Y_{vis} is limited to low values due to particles which escape detection. The data are compared to Monte Carlo predictions, normalised to the number of data events.

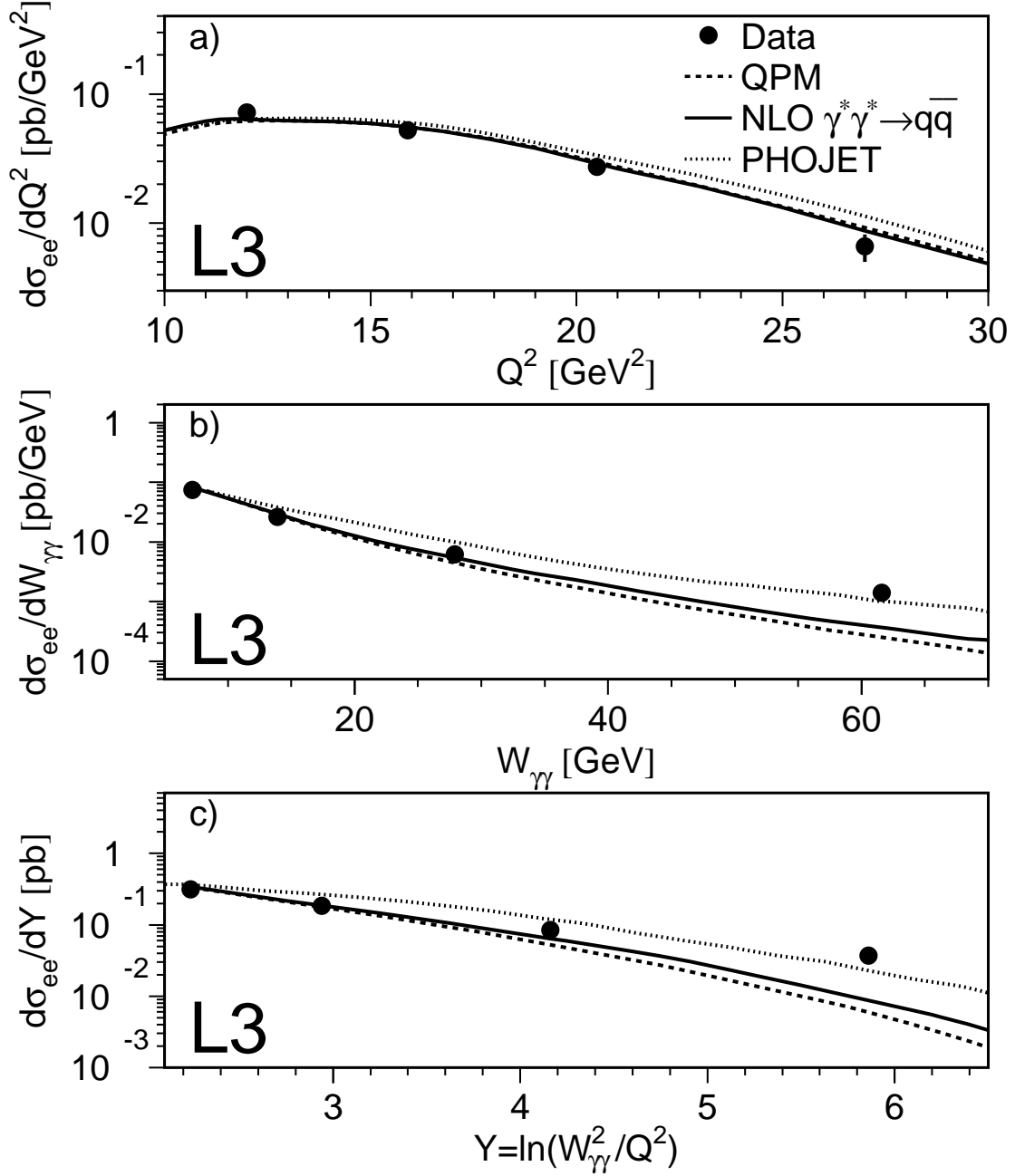


Figure 5: The differential cross sections of the $e^+e^- \rightarrow e^+e^- \text{ hadrons}$ process, in the kinematical region defined in the text, after applying QED radiative corrections, as a function of a) Q^2 , b) $W_{\gamma\gamma}$ and c) Y . The LO and NLO predictions [12] for the process $\gamma^*\gamma^* \rightarrow q\bar{q}$ are displayed as the dashed and solid lines respectively. The dotted line shows the prediction of the PHOJET Monte Carlo.

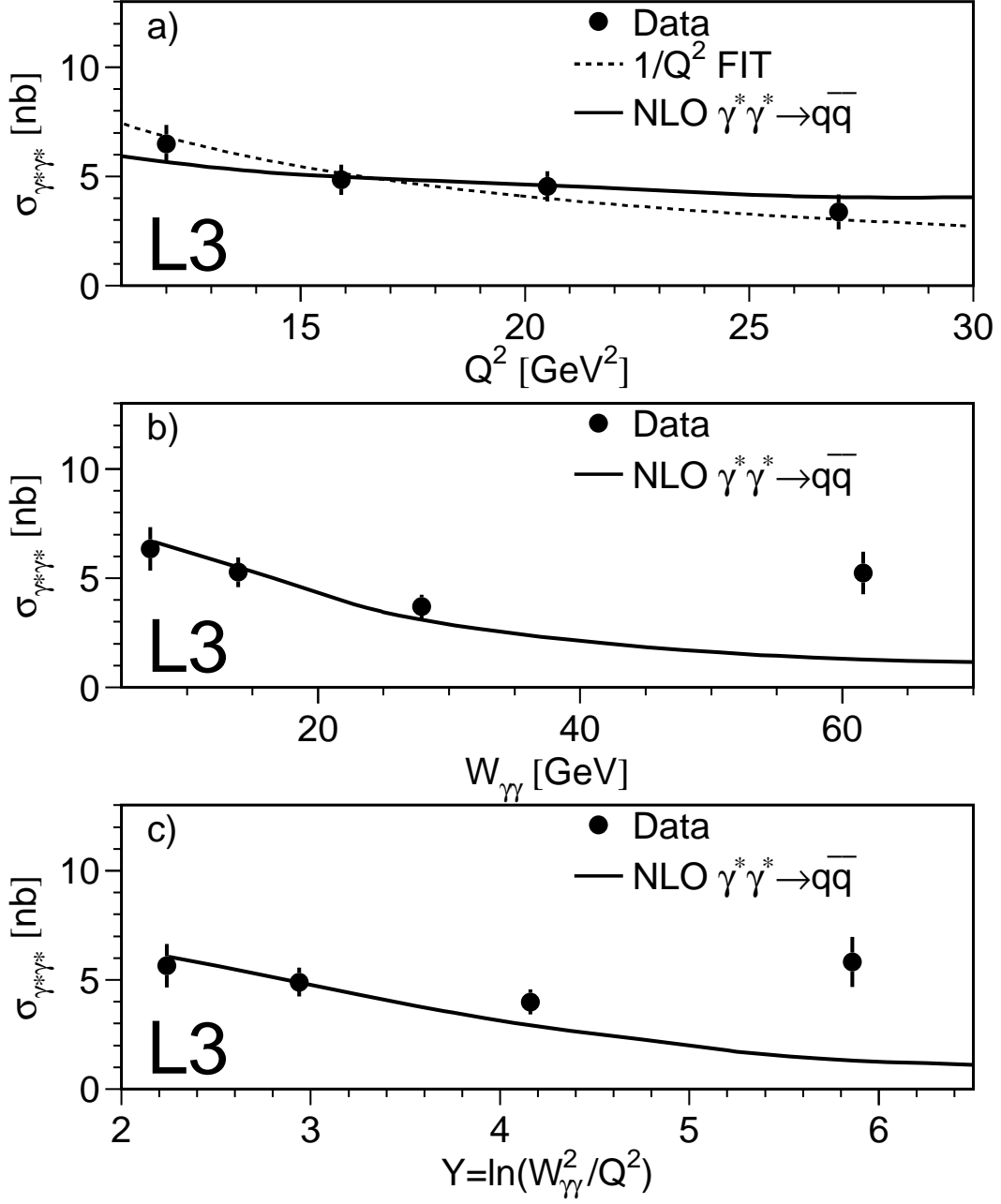


Figure 6: Cross sections of the $\gamma^*\gamma^* \rightarrow \text{hadrons}$ processes as a function of a) Q^2 , b) $W_{\gamma\gamma}$, and c) Y in the kinematical region defined in the text, after applying QED radiative corrections. The dashed line represents the fit to the data described in the text. The NLO predictions of Reference 12 for the process $\gamma^*\gamma^* \rightarrow q\bar{q}$ are displayed as a solid line.